Resonant ultrasound spectroscopy

1997 J. Phys.: Condens. Matter 9 6001

(http://iopscience.iop.org/0953-8984/9/28/002)

J. Phys.: Condens. Matter **9** (1997) 6001–6029. Printed in the UK PII: S0953-8984(97)71630-8

REVIEW ARTICLE

Resonant ultrasound spectroscopy

R G Leisure and F A Willis

Department of Physics, Colorado State University, Fort Collins, CO 80523, USA

Received 8 April 1997

Abstract. Resonant ultrasound spectroscopy (RUS) involves the study of the mechanical resonances of solids. The resonant response of a particular object depends on its shape, elastic constants, crystallographic orientation, density, and dissipation. It is possible to obtain the complete elastic constant matrix of relatively low-symmetry materials from a RUS spectrum on a single small sample (<1 mm^3). The measurement and the computation of the RUS spectra of solids are reviewed. Several examples of the use of the technique are discussed.

Contents

1. Introduction

Ultrasonic measurements have been valuable for the study of condensed matter physics and materials science. Such measurements provide the most accurate characterization of the elasticity of solids, and are a sensitive probe of any entity in the material which couples to long-wavelength phonons. The usual measurement techniques, although quite powerful, suffer from certain limitations which have prevented a more widespread use. Among the

most important restrictions are the following: relatively large samples are required for accurate measurements; a number of independent measurements, often on separate samples, are needed to fully characterize the elastic properties of a material. This number may be rather high for low-symmetry materials. Recently a new technique, resonant ultrasound spectroscopy (RUS), has been demonstrated [1–4]. This new technique drastically reduces the amount of material required for accurate results. In addition, the elastic properties may be fully characterized by one spectrum on one sample, which results in a significant saving in sample preparation time. Finally, the intrinsic accuracy of the new method is high. These advantages are partially offset by a reliance on computer programs to extract the basic physical quantities from the data. While the computing requirements would be a serious concern with the computers of a decade ago, the power of desk top computers today is adequate for data reduction, and one may expect the situation to become even better in the future. Recent theoretical advances mean that in principle the technique can be applied to any well defined sample shape, and to materials with any crystallographic symmetry.

Ultrasonic measurements may be regarded as a type of elastic wave spectroscopy. The spectra are rather rich, due in part to the anisotropic nature of elasticity in crystals. The kinds of information obtained are readily understood by considering a common situation. The velocity and attenuation of ultrasonic waves are often measured. The elastic constants of the material may be derived from the velocity measurements. The elastic constants are of fundamental importance; they are the second derivatives of the free energy with respect to strain and are directly related to the atomic bonding of the material. In addition, they are connected to thermal properties of solids through the Debye theory. In combination with specific heat and thermal expansion measurements, elastic constant data can be used to determine the equation of state and various thermodynamic functions. While the elastic constants represent primarily equilibrium thermodynamics, the attenuation is a manifestation of irreversible processes. The attenuation may be due to energy absorption by various physical entities in the material such as conduction electrons, thermal phonons, defects, order parameter relaxation, etc. Perhaps less interesting, attenuation may arise due to scattering or beam spreading.

As will be described below, RUS offers significant advantages over earlier methods of ultrasonic spectroscopy. In what follows we will provide a short review of elastic waves in condensed matter and discuss briefly previous ultrasonic techniques. The new technique of RUS will be described including a review of the theoretical basis of the method. Examples of results obtained by RUS will be given to illustrate the power of the technique. We will not attempt to be exhaustive in our coverage of this subject, but will rely on references to the literature to complete the picture.

2. Ultrasonic waves in condensed matter

2.1. Crystalline elasticity

Materials are generally deformed when forces are applied. If we denote by $u_i(x_k), i, k = 1, 2, 3$, the displacement of a point whose coordinates were x_k before the deformation, the deformation may be described by a strain tensor

$$e_{kl} = \frac{1}{2}\left[\frac{\partial u_k}{\partial x_l} + \frac{\partial u_l}{\partial x_k}\right] \tag{1}$$

where it is assumed that the strains are small so that second-order terms may be neglected. The diagonal elements of the strain tensor, e_{kk}, are a measure of the extension per unit

length of the kth axis, while the off-diagonal elements, e_{kl}, are a measure of the change in the angle between the k and l axes. The forces related to the deformation are described in terms of the stress tensor σ_{ij} where the subscript i denotes the ith component of a force acting on a unit area with normal along the jth axis. For linear elasticity a generalized Hooke's Law holds so that

$$\sigma_{ij} = C_{ijkl}e_{kl} \tag{2}$$

where the C_{ijkl} are the elastic constants. It can be shown that the elastic constants are the second derivatives of the free energy with respect to strain [5, 6]. We use the convention that repeated indices are to be summed over. Hence, it appears that there are 81 independent elastic constants. However, a considerable simplification is possible. With the assumption that no net body torques act on the material it can be shown [5, 6] that $\sigma_{ij} = \sigma_{ji}$, thus i and j may be interchanged. It is obvious that k and l can be interchanged in (1). As a result, the number of independent elastic constants is reduced to 36. Finally, the condition that the strain energy be a function only of the state of the material leads to $C_{ijkl} = C_{klij}$, which reduces the number of independent elastic constants to 21. Any further reductions depend on the symmetry of the crystal under consideration. Only the lowest-symmetry crystal, triclinic with a onefold axis of rotation, has 21 elastic constants. Mirror planes, n-fold rotation axes, etc can reduce the number considerably. For example, a single crystal with cubic symmetry has only three independent elastic constants and an isotropic material has only two.

The equations of motion are obtained by considering the forces acting on an infinitesimal cube of material of volume $\mathrm{d}x\,\mathrm{d}y\,\mathrm{d}z$. Neglecting body forces, the net force is due to the different stresses acting on different faces of the cube, i.e. it is due to the spatial variation of the stress. Newton's second law for the cube becomes

$$\partial\sigma_{ij}/\partial x_j = \rho\partial^2 u_i/\partial t^2 \tag{3}$$

where ρ is the mass density. Combining (1)–(3) and using $C_{ijkl} = C_{ijlk}$ gives for the equation of motion

$$C_{ijkl}\partial^2 u_k/(\partial x_j \partial x_l) = \rho\partial^2 u_i/\partial^2 t. \tag{4}$$

The solutions of (4) are in general quite difficult. In large measure, this difficulty has dictated experimental techniques. An approach widely used is to assume plane wave solutions for (4) and then to design experiments so that, to a reasonable approximation, the waves propagated are planar. This is the usual situation for the pulse-echo and continuous-wave methods to be described in the next section.

2.2. Plane-wave propagation methods

The pulse-echo technique is a widely used method to obtain ultrasonic velocity and attenuation data for solids [7]. The experimental arrangement is shown in figure 1. The sample to be studied is prepared with two flat and parallel faces, usually oriented perpendicularly to a major crystallographic axis. Piezoelectric transducers are bonded to one, or both, faces. An electromagnetic pulse generates a short train of ultrasonic vibrations at the transmitting transducer which then travel back and forth across the sample. The 'echoes' excite the receiving transducer (which can be the same as the transmitting transducer) as the pulse reverberates in the sample. With corrections for transducer effects, the ultrasonic velocity is determined from the time of flight and the sample thickness. The attenuation is determined from the decay of the echo amplitude with time.

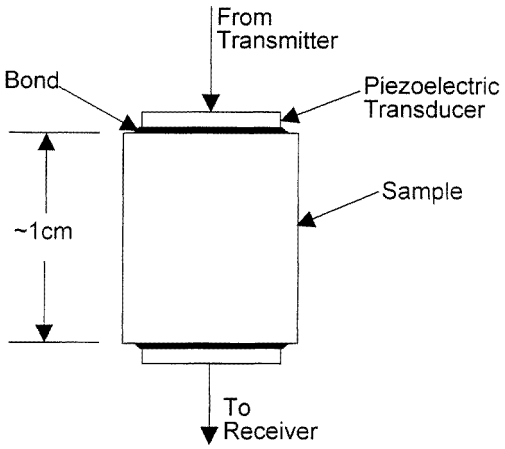

Figure 1. A sample–transducer arrangement for conventional ultrasonic measurements.

Although less well known than the pulse-echo technique, continuous-wave methods have been used successfully to make sensitive attenuation and velocity measurements [8]. The sample–transducer arrangement is the same as that of figure 1. The transmitting transducer is driven continuously and a resonant response is observed at frequencies corresponding to the sample length being some multiple of a half-wavelength of sound. With transducer corrections, the ultrasonic wave velocity is determined from the measured resonant frequencies. The attenuation is determined from the Q of the resonance lines.

Both the pulse-echo and continuous-wave methods above almost always rely on the assumption of plane waves to interpret the results. Plane-wave solutions of (4) have been given for the various crystal symmetries [9, 10] and the relations between the ultrasonic velocity and elastic constants obtained. These relations are fairly simple for cubic materials, but become increasingly complicated for lower-symmetry crystals. For cubic materials it is possible to obtain the three independent elastic constants by propagating one longitudinal and two independent transverse waves along the [110] crystalline axis. Thus, three measurements along this axis give the three elastic constants. For orthorhombic symmetry, nine measurements along six different directions are needed to determine the complete elastic constant tensor, a laborious task. Nevertheless, both the pulse-echo and the continuous-wave approach offer quick, easily interpretable methods for elastic constant measurements on high-symmetry materials. Both methods can be extended to rather high frequencies. However, the methods have several deficiencies which are well known to practitioners.

(i) Relatively large samples are required due to the need to approximate plane-wave propagation. First of all, the diameter of the transducer must be much greater than the wavelength of ultrasound in the sample. For frequencies in the 10 MHz range this requirement leads to typical transducer diameters of 1 cm. Diffraction will still lead to beam spreading, so, to avoid reflections from the sides of the sample, the sample diameter must be somewhat larger than the transducer diameter.

(ii) Near the transducer the wave is approximately planar, but diffraction effects exist and limit the accuracy of velocity and attenuation measurements [11].

(iii) There are several deleterious effects associated with bonding a transducer to the face of the sample. Coupling losses in the bonding agent often affect the results. The bonding agent may introduce non-parallelism of the end faces. These effects are all compounded by

the fact that the usual transducer is phase sensitive; the voltage out is proportional to the sum of the *amplitudes*, not the intensities, of the various waves impinging across the face of the transducer. It is possible to obtain cancellation effects due to uninteresting factors which reduce the detected signal.

(iv) As discussed above, the number of independent measurements that must be made to determine the complete set of elastic constants is at least equal to the number of elastic constants to be determined. For symmetries lower than cubic, measurements along more than one crystallographic axis must be made. In addition to being time consuming, these independent measurements compromise the relative accuracy with which the elastic constants are known. Many materials of current interest have symmetries much lower than cubic; thus, it is often impractical to obtain the full set of elastic constants by the usual techniques.

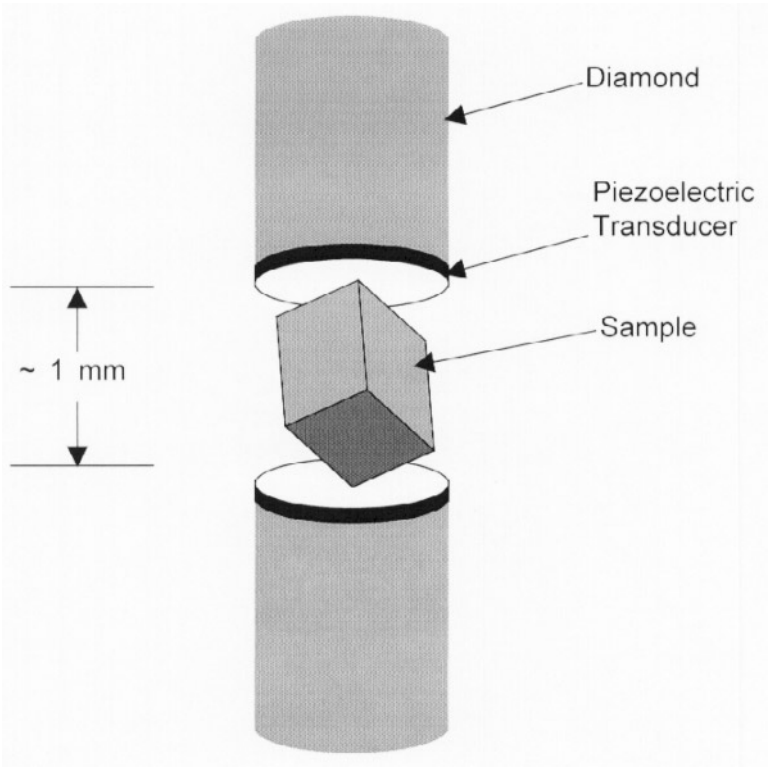

Figure 2. A sample–transducer arrangement for RUS.

3. Resonant ultrasound spectroscopy

RUS offers an approach which differs fundamentally from the more conventional methods just described. RUS does not rely on the plane-wave approximation; indeed there are no plane waves. Instead, RUS is based on the measurement of the vibrational eigenmodes of samples of well defined shapes, usually parallelepipeds or spheres. A typical experimental arrangement is illustrated in figure 2. A sample, often a parallelepiped, is held lightly between two piezoelectric transducers. The sample is excited at one point by one of the

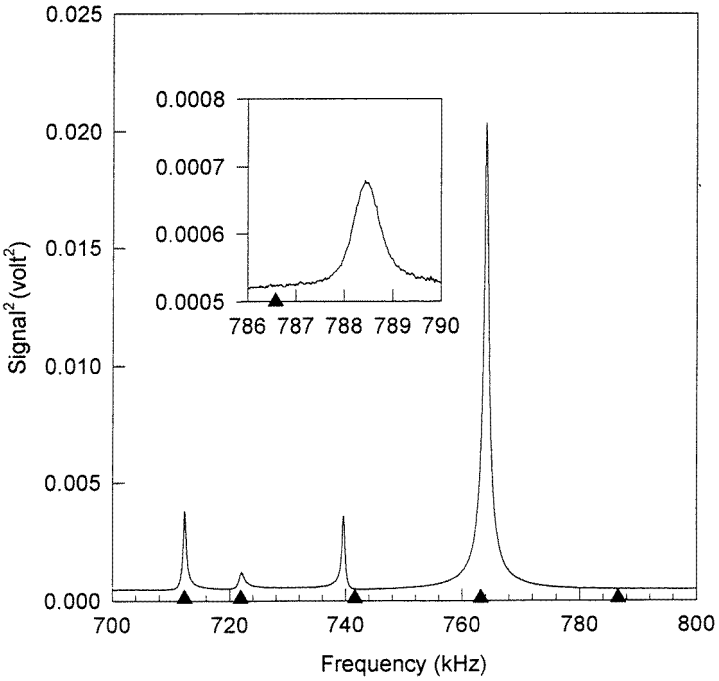

Figure 3. An RUS spectrum for a textured, polycrystalline copper parallelepiped of dimensions $2.016 \times 2.172 \times 1.810$ mm^3. The inset shows the resonance at 788.5 kHz after the sample was remounted in the holder. The arrows indicate the computed frequencies based on a fit to the first 50 resonances with an rms error of 0.2%.

transducers. The frequency of this driving transducer is swept through a range corresponding to a large number of vibrational eigenmodes of the sample. The resonant response of the sample is detected by the opposite transducer. A large response is observed when the frequency of the driving transducer corresponds to one of the sample eigenfrequencies. A segment of a typical spectrum is shown in figure 3. As will be discussed below, the eigenfrequencies depend on the elastic constants, the sample shape, the orientation of the crystallographic axis with respect to the sample, and the density. By measuring a large number of resonant frequencies on one sample it is possible to obtain information about all these quantities. (The square of the frequencies depends on the product of the elastic constants and the linear dimensions of the sample; thus, elastic constants and linear dimensions cannot be determined independently.) Usually the sample shape, crystallographic orientation, and density are known and one determines the complete elastic constant matrix from such a spectrum. There is no need to prepare a different sample with different crystalline orientations.

Accurate measurements of the sample eigenfrequencies require attention to a number of critical parameters. These parameters have been discussed in detail by Migliori *et al* [4]; thus, the present discussion will only outline the key factors. Ideally the sample shape would be known perfectly, there would be no external forces acting on the sample, and the methods used to excite and detect the resonances would not affect the measured frequencies. In practice the ideal conditions can be approached closely enough that elastic constant measurements are of exceptionally high absolute accuracy [4, 12].

The computation of the eigenfrequencies to be discussed below is for a sample of well defined shape, usually a rectangular parallelepiped or a sphere, although cylinders have also been used [13]. Detailed methods for preparing accurate parallelepipeds have been given by Migliori *et al* [4]. Methods are also available for preparing spheres [14]. A complete analysis of the error introduced by a deviation from the assumed shape is difficult and a simple formula for estimating such error is not available [15]. However, absolute accuracies for the elastic constants range from about 3% for off-diagonal moduli to about 0.02% for some of the pure shear moduli.

Transducers used to excite and detect the sample eigenfrequencies often have resonant responses. In such cases, the detected resonance is a combination of the sample response and the transducer response with the result that the observed frequency may be either higher or lower than the true sample eigenfrequency. Figure 2 includes a schematic diagram of the Migliori transducer design [4, 16] which overcomes this problem. The bare lithium niobate piezoelectric transducer has a fundamental compressional mode frequency of 30 MHz; however, the bending mode frequency is much lower. By bonding the transducer to a cylinder of diamond, which has an exceptionally high sound velocity, all resonant frequencies of the transducer–diamond assembly are higher than 4 MHz. Most materials with dimensions $\sim$ 1 mm have many resonances below 4 MHz, thus this design permits the measurement of the sample eigenfrequencies with essentially no shift due to the transducer frequency response. Transducer designs based on polyvinylidene fluoride films [3] and ferromagnetic films [17] have also been given.

With non-resonant transducers, the signal voltage is rather low. This problem can be compounded by capacitative loading by the coaxial line used to carry the signal from the experimental environment to the receiver. This effect depends on the length of coaxial line and the characteristics of the receiver. Low-noise amplifiers and proper attention to input impedance are needed for good results. Finally, the theoretical solutions discussed below are for free boundaries. The transducers apply some force to the sample, so the boundaries are not entirely free. It has been found [4] that if the force applied by the transducer is 0.01 N or less, and the drive voltage is kept low, the shift in eigenfrequencies resulting from this force is of the order of parts per million. Instrumentation is now available commercially [18, 19] which solves many of the experimental problems.

It is apparent that RUS overcomes many of the deficiencies of the more conventional methods for the measurement of elastic constants.

(i) Small samples are naturally accommodated. Sample dimensions of approximately 1 mm typically result in many eigenfrequencies below 4 MHz, a convenient range. Compared to more conventional methods described above, the minimum sample volume is reduced by roughly three orders of magnitude. Many novel materials, especially in single-crystal form, are only available as small samples, thus this reduction in minimum size vastly expands the range of materials susceptible to precise ultrasonic measurements.

(ii) There are no diffraction effects to worry about; there is no plane-wave approximation. The inherent accuracy is high.

(iii) There is no bond between the transducer and the sample, only contact force is used. With sensitive electronics, a very low contact force is possible so that transducer loading effects are negligible. The absence of a bond is very useful for temperature dependent measurements because differential thermal contraction often leads to bonds breaking, or at best strains being applied to the sample under investigation. This absence of a bond is especially important near phase transitions.

(iv) All of the elastic constants are determined from one spectrum. There is no need

to prepare a sample for measurements along a different crystalline direction. As a result, high relative accuracy for the elastic constants is obtained. Low-symmetry materials are accommodated almost as easily as high-symmetry materials.

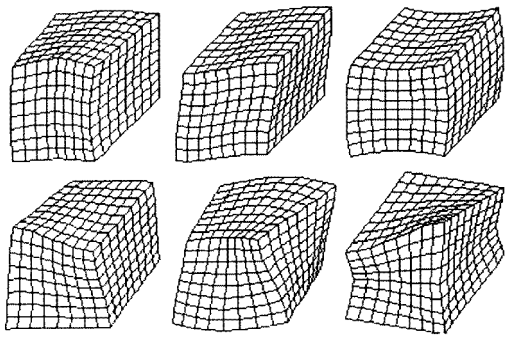

Figure 4. An illustration of several vibrational eigenmodes for a rectangular parallelepiped.

Given the advantages of RUS just listed, one might wonder why this technique did not supplant the more conventional techniques for modulus measurements long ago. A major reason is that the vibrational eigenmodes of a three-dimensional object are rather complicated. Examples of calculated eigenmodes are shown in figure 4. A RUS spectrum contains much information, but extracting all that information is not a simple task. The procedure is to compare the measured frequencies with computed frequencies which are calculated with an initial set of input parameters. The input parameters for the computation are varied in an iterative process to obtain good agreement between measured and computed frequencies, and in this way the input parameters are determined. Usually the input parameters are the elastic constants, although parameters describing crystalline orientation or sample shape can be used. Thus, an essential ingredient of RUS is the ability to calculate the eigenfrequencies in an efficient manner and systematically iterate toward a match of the measured and computed frequencies. The computational methods have been developed by Holland [20], Demarest [21], Ohno *et al* [22, 23], Visscher *et al* [24], and Migliori *et al* [4] and will be outlined in the next section. As will be shown below, the calculations involve finding the eigenvalues and eigenvectors of a large matrix. To find the elastic constants, the calculation has to be repeated many times in an iterative process. For good accuracy the size of the matrix is typically 858×858, although exploitation of symmetry can reduce the problem dramatically. Until relatively recently such computations required large computers, but it is now feasible to perform these calculations on PC type computers. The continued increase in computing speed means that the computational aspect of the problem is no longer a limitation.

4. Theoretical basis of RUS

4.1. Computation of the eigenfrequencies

An integral element of RUS is comparison of measured and computed frequencies. The direct approach would be to solve (4); however, an exact solution for a 3D object remains unsolved, except for some highly special cases. An approximate solution is needed. Equation (4) is not the most convenient starting point for such an approximation.

Fortunately, it turns out [24] that the displacements $u_i(x_k)$ which are a solution of (4) with free boundaries are exactly those for which the elastic Lagrangian is an extremum. This fact leads to the following general scheme. The displacements are expanded in some suitable set of basis functions. The derivatives of the Lagrangian with respect to the expansion coefficients are equated to zero to determine the extremum. This leads to a generalized eigenvalue problem in which kinetic and potential energies are represented by rather large matrices. The eigenvalues give the square of the resonant frequencies and the eigenvectors conveniently give the displacements. Thus, the numerical part of RUS consists of calculating a large matrix, finding the eigenvalues, and then using the eigenvectors to calculate 'corrections' to the set of input parameters so as to iterate toward a match between computed and measured frequencies. The remainder of this section is broken up into three parts: the calculation of the eigenvalues and eigenvectors; the inverse problem of determining material parameters from the measured frequencies; and a brief discussion of dissipation.

4.1.1. The general computational method. The derivation starts with the Lagrangian for a 3D elastic body,

$$L = \frac{1}{2}\int_V (\rho\omega^2 u_i^2(\boldsymbol{r}) - C_{iji'j'}u_{i,j}(\boldsymbol{r})u_{i',j'}(\boldsymbol{r}))\,\mathrm{d}V \tag{5}$$

where an $\exp(\mathrm{i}\omega t)$ time dependence has been assumed. The subscripts are to be summed over, $i, j, i', j' = 1, 2, 3$, and subscripts separated by commas denote a differentiation with respect to the subscripts appearing on the right-hand side of the comma. It is useful to expand the displacements appearing in (5) in some basis such as

$$u_i(\boldsymbol{r}) = a_{i\alpha}\Phi_\alpha(\boldsymbol{r}) \tag{6}$$

where $a_{i\alpha}$ are the expansion coefficients and $\Phi_\alpha(\boldsymbol{r})$ are the basis functions. The $\Phi_\alpha(\boldsymbol{r})$ are often chosen based on the shape of the sample. In particular, it is important to be able to integrate the basis functions and their derivatives over the volume of the sample. For parallelepipeds, a convenient choice for $\Phi_\alpha(\boldsymbol{r})$ is the Legendre polynomials [21, 22], while a series expansion in powers of x, y, and z, i.e. $x^l y^m z^n$ where l, m, and n are integers, is useful for a variety of shapes [24]. Each of the three components of the displacement is expanded as in (6) and each has its own set of expansion coefficients. Substituting (6) into the Lagrangian gives

$$L = \frac{1}{2}\left(a_{i\alpha}a_{i'\alpha'}\rho\omega^2\int_V \delta_{ii'}\Phi_\alpha(\boldsymbol{r})\Phi_{\alpha'}(\boldsymbol{r})\,\mathrm{d}V - a_{i\alpha}a_{i'\alpha'}\int_V C_{iji'j'}\Phi_{\alpha,j}(\boldsymbol{r})\Phi_{\alpha',j'}(\boldsymbol{r})\,\mathrm{d}V\right). \tag{7}$$

This can be more compactly rewritten as

$$L = \tfrac{1}{2}((\rho\omega^2)\boldsymbol{a}^T\mathbf{E}\boldsymbol{a} - \boldsymbol{a}^T\boldsymbol{\Gamma}\boldsymbol{a}) \tag{8}$$

in which the integrals appearing in (7) are now the elements of the matrices $\mathbf{E}$ and $\boldsymbol{\Gamma}$ and the expansion coefficients, $a_{i\alpha}$, are vectors. Requiring L to be an extremum is accomplished by setting the derivatives of L with respect to each of the expansion coefficients equal to zero. The result is a generalized eigenvalue equation

$$\boldsymbol{\Gamma}\boldsymbol{a} = (\rho\omega^2)\mathbf{E}\boldsymbol{a}. \tag{9}$$

The eigenvalues are $\lambda = \rho\omega^2$ and the eigenvectors, $\boldsymbol{a}$, are the expansion coefficients. Thus, calculating the resonant frequencies for a 3D elastic body is essentially one of calculating $\boldsymbol{\Gamma}$ (and $\mathbf{E}$ if needed) and finding the eigenvalues of (9). It will be seen later that the

eigenvectors are also useful in fitting the calculated resonant frequencies with the measured values.

The elements of $\mathbf{E}$ and $\mathbf{\Gamma}$ are calculated using two terms from the expansion of $\boldsymbol{u}(\boldsymbol{r})$ given in (6). For example, for a rectangular parallelepiped and normalized Legendre polynomials ($\bar{P}_n(x) = \sqrt{(2n+1)/2}P_n(x)$ where P_n are the usual Legendre polynomials) as the basis functions, the expansion of the displacement becomes

$$\boldsymbol{u}(\boldsymbol{r}) = \frac{a_{i\lambda\mu\nu}}{\sqrt{L_1L_2L_3}}\bar{P}_\lambda(X)\bar{P}_\mu(Y)\bar{P}_\nu(Z)\hat{e}_i$$
$$X = x/L_1 \qquad Y = y/L_2 \qquad Z = z/L_3. \tag{10}$$

Here, $i = 1, 2, 3$ corresponds to the x, y, z components of $\boldsymbol{u}(\boldsymbol{r})$, the e_i are the usual unit vectors, the sample dimensions in the x, y, and z directions are $2L_1$, $2L_2$, and $2L_3$ respectively, and we use the reduced coordinates X, Y, and Z. Equating p with a set $i\lambda\mu\nu$ and q with a set $i'\lambda'\mu'\nu'$ allows one to calculate the matrices. The elements of $\mathbf{E}$ and $\mathbf{\Gamma}$ are thus given by

$$E_{pq} = \delta_{ii'}\int_{-1}^{+1}\int_{-1}^{+1}\int_{-1}^{+1}\bar{P}_\lambda(X)\bar{P}_{\lambda'}(X)\bar{P}_\mu(Y)\bar{P}_{\mu'}(Y)\bar{P}_\nu(Z)\bar{P}_{\nu'}(Z)\,\mathrm{d}X\,\mathrm{d}Y\,\mathrm{d}Z \tag{11}$$

and

$$\mathbf{\Gamma}_{pq} = \sum_{j=1}^{3}\sum_{j'=1}^{3}\frac{C_{iji'j'}}{L_jL_{j'}}\int_{-1}^{+1}\int_{-1}^{+1}\int_{-1}^{+1}\frac{\partial(\bar{P}_\lambda(X)\bar{P}_\mu(Y)\bar{P}_\nu(Z))}{\partial X_j}$$
$$\times\frac{\partial(\bar{P}_{\lambda'}(X)\bar{P}_{\mu'}(Y)\bar{P}_{\nu'}(Z))}{\partial X_{j'}}\,\mathrm{d}X\,\mathrm{d}Y\,\mathrm{d}Z. \tag{12}$$

The nine terms in (12) are given by Ohno [22] as $G_1, G_2, \ldots, G_9$ for the case of parallelepipeds. The reader is cautioned that an apparent typographical error exists in Ohno's paper for his equation (11) for the $(i, i') = (3, 3)$ block of $\mathbf{\Gamma}$.

In order that the rank of $\mathbf{E}$ and $\mathbf{\Gamma}$ remain finite, the series for the expansion of $\boldsymbol{u}(\boldsymbol{r})$ must be truncated at some point. This is usually accomplished [24] by requiring

$$\lambda + \mu + \nu \leqslant R \tag{13}$$

where R is some integer. It can be shown [25] that this condition leads to

$$N = (R+1)(R+2)(R+3)/6 \tag{14}$$

combinations of (λ, μ, ν) in the expansion. The rank of the matrices will be $3N$ because each component of the displacement will have N terms in the expansion. It has been found [24] that $R = 10$ is generally a good compromise between accuracy and computational overhead. Even using $R = 10$ leads to an 858×858 matrix.

The form of the matrices depends on the order in which the expansion in (10) is written. Writing the expansion in a different order in effect swaps rows and columns in the matrix. As can be seen from (11), if the sample shape is a parallelepiped with the faces perpendicular to the x, y, z directions and the displacement is expanded in Legendre polynomials, $\mathbf{E}$ is simply the identity matrix. However, if the displacement is expanded in a power series of xyz, $\mathbf{E}$ will be more complicated. Thus, there is an advantage in expanding the displacement in terms of Legendre polynomials for parallelepipeds. Likewise, using a power series of xyz for other sample shapes, such as spheres and cylinders, may be more convenient due the ease in which the integrals may be performed.

To summarize, calculating the vibrational eigenfrequencies of a sample involves solving (9) with a suitable choice of basis functions and an appropriate truncation of the expansion of (10). The matrix elements are given by (11) and (12) for the case of a rectangular

parallelepiped and normalized Legendre polynomials as the basis functions. There are standard FORTRAN routines for solving such eigenvalue problems.

4.1.2. Use of symmetry to speed the calculations. It was realized by Holland [20] and Demarest [21] that if the sample shape and elastic constant matrix had common symmetry elements the matrices involved in calculating the resonant frequencies could be factored into two, or more, smaller matrices. Ohno [22] has an excellent treatment of the use of symmetry to split the matrices. This section will elaborate on his work. The ability to factor the problem into a series of smaller problems is significant in that the time needed to solve for the eigenvalues and eigenvectors of a matrix is commonly taken to be proportional to the number of elements of the matrix. The need to solve multiple smaller matrices is more than compensated by being able to work with smaller matrices. It has been found in practice that, due to the large size of the original problem, the actual time saved is somewhat more than expected.

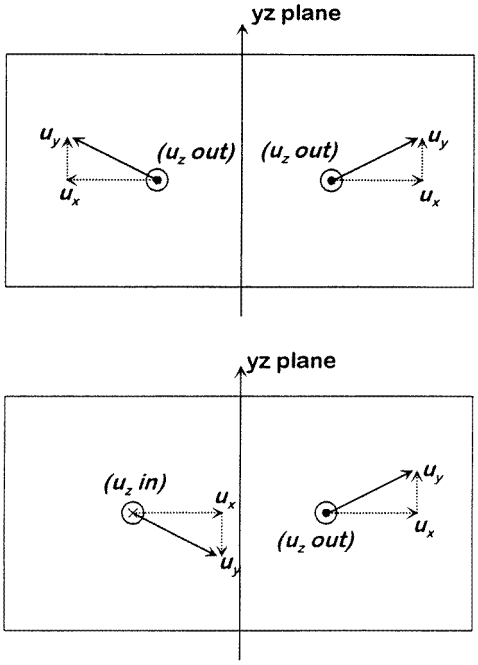

Figure 5. An illustration of symmetric and antisymmetric displacement functions for mirror plane symmetry.

To see the effects of symmetry we start by considering a parallelepiped with a yz mirror plane. Following Ohno, it is convenient to group the displacement functions as to whether they are symmetric or antisymmetric under a reflection in the yz plane. These two types of displacement function are illustrated in figure 5. For a symmetric function, a reflection in this plane changes the sign of u_x, but does not change the signs of u_y and u_z. The antisymmetric function behaves oppositely on reflection: the sign of u_x does not change, but the signs of u_y and u_z do. Since the Lagrangian represents the kinetic and potential energies, it will be invariant under the symmetry operations of the crystal, and it is obviously invariant under a sign change of $\boldsymbol{u}(\boldsymbol{r})$. Thus, the x components of the symmetric

modes, u_x, have odd parity with respect to x, while the y and z components, u_y and u_z, are even in x. Likewise, it is seen for the antisymmetric modes that u_x has even parity with respect to x and u_y and u_z have odd parity. The y and z coordinates do not change sign under a yz mirror plane reflection; thus, the displacement functions need have no definite parity with respect to these coordinates. It was stated in the preceding section that the form of the matrices will be dependent upon the manner in which the expansion of the displacement is written. If one naively writes the expansion for a parallelepiped with a yz mirror plane, as given in (10), in numerical order of (λ, μ, ν), it will be found that a large number of matrix elements will be identically equal to zero. Unfortunately the zeros will be scattered haphazardly throughout $\mathbf{\Gamma}$ resulting in a sparsely populated matrix. It is much more convenient to write the expansion in terms of a symmetric part and an antisymmetric part

$$\boldsymbol{u}(\boldsymbol{r}) = \boldsymbol{u}^s(\boldsymbol{r}) + \boldsymbol{u}^a(\boldsymbol{r}) \tag{15}$$

where

$$\begin{aligned}
\boldsymbol{u}^s(\boldsymbol{r}) = \frac{1}{\sqrt{L_1L_2L_3}}\Bigg(& \sum_{\substack{\lambda\mu\nu \\ \lambda=odd}} a_{1\lambda\mu\nu}\bar{P}_\lambda(X)\bar{P}_\mu(Y)\bar{P}_\nu(Z)e_1 \\
& + \sum_{\substack{\lambda\mu\nu \\ \lambda=even}} a_{2\lambda\mu\nu}\bar{P}_\lambda(X)\bar{P}_\mu(Y)\bar{P}_\nu(Z)e_2 + \sum_{\substack{\lambda\mu\nu \\ \lambda=even}} a_{3\lambda\mu\nu}\bar{P}_\lambda(X)\bar{P}_\mu(Y)\bar{P}_\nu(Z)e_3\Bigg) \\
\boldsymbol{u}^a(\boldsymbol{r}) = \frac{1}{\sqrt{L_1L_2L_3}}\Bigg(& \sum_{\substack{\lambda\mu\nu \\ \lambda=even}} a_{1\lambda\mu\nu}\bar{P}_\lambda(X)\bar{P}_\mu(Y)\bar{P}_\nu(Z)e_1 \\
& + \sum_{\substack{\lambda\mu\nu \\ \lambda=odd}} a_{2\lambda\mu\nu}\bar{P}_\lambda(X)\bar{P}_\mu(Y)\bar{P}_\nu(Z)e_2 + \sum_{\substack{\lambda\mu\nu \\ \lambda=odd}} a_{3\lambda\mu\nu}\bar{P}_\lambda(X)\bar{P}_\mu(Y)\bar{P}_\nu(Z)e_3\Bigg).
\end{aligned} \tag{16}$$

It is obvious that the entire expansion is still present; only the ordering of the terms has been changed. While this may seem like an unnecessary complication, it does have the very great advantage of automatically factoring $\mathbf{\Gamma}$ into four large blocks. It will be shown below that terms from the symmetric portion of the expansion only couple with other symmetric terms. Likewise, antisymmetric terms only couple with other antisymmetric terms. The final result is that $\mathbf{\Gamma}$ is split into four blocks. The matrix elements corresponding to symmetric–antisymmetric terms are zero. If the terms are written as in (15), the top left quarter of $\mathbf{\Gamma}$ will, in general, be filled with non-zero values corresponding to symmetric terms coupling with other symmetric terms and the bottom right corner of $\mathbf{\Gamma}$ will be filled with non-zero terms corresponding to antisymmetric terms coupling with other antisymmetric terms. The two remaining blocks, approximately one-half of the entire matrix, will be filled with zeros.

It is easy to take advantage of the mirror plane symmetry to reduce the computation time. Rather than calculating one large matrix with non-zero blocks along the diagonal, two smaller matrices can be calculated separately. Using the example above, the first matrix is calculated using only combinations of (λ, μ, ν) from the symmetric part of the expansion and its eigenvalues and eigenvectors determined. The process is then repeated using the combinations of (λ, μ, ν) from the antisymmetric part of the expansion and a second set of eigenvalues and eigenvectors obtained. The two sets of eigenvalues and eigenvectors can then be combined and sorted in ascending order of eigenvalues. Thus, we can now calculate individually the eigenvalues and eigenvectors of the two relatively small blocks

corresponding to the two types of displacement. This results in the calculations being much faster, and also provides a means of categorizing the mode types.

A single mirror plane was used to split the displacement into symmetric and antisymmetric portions as given by (15) and (16). If additional symmetry operations are included, the displacement can be factored again. For example, if the sample has a second mirror plane parallel to the xz plane, each of the symmetric and antisymmetric parts of (16) can be factored, resulting in four terms. In this example, an xz mirror plane will transform the y coordinate, resulting in a restriction on μ. The result can be written in a form similar to (15), but with two superscripts.

$$\boldsymbol{u}(\boldsymbol{r}) = \boldsymbol{u}^{ss}(\boldsymbol{r}) + \boldsymbol{u}^{sa}(\boldsymbol{r}) + \boldsymbol{u}^{as}(\boldsymbol{r}) + \boldsymbol{u}^{aa}(\boldsymbol{r}). \tag{17}$$

Now the first superscript refers to the parity of the displacement with respect to the first symmetry operation and the second superscript refers to the parity with respect to the second symmetry operation. Using the second term in (17), $\boldsymbol{u}^{SA}(\boldsymbol{r})$, as an example, we want terms that are symmetric with respect to a yz mirror plane and antisymmetric with respect to a xz mirror plane. Terms in the displacement satisfying these requirements are

$$\begin{aligned}\boldsymbol{u}^{sa}(\boldsymbol{r}) = \frac{1}{\sqrt{L_1L_2L_3}}\Bigg(&\sum_{\substack{\lambda\mu\nu \\ \lambda=odd \\ \mu=odd}} a_{1\lambda\mu\nu}\bar{P}_\lambda(X)\bar{P}_\mu(Y)\bar{P}_\nu(Z)e_1 \\ &+ \sum_{\substack{\lambda\mu\nu \\ \lambda=even \\ \mu=even}} a_{2\lambda\mu\nu}\bar{P}_\lambda(X)\bar{P}_\mu(Y)\bar{P}_\nu(Z)e_2 + \sum_{\substack{\lambda\mu\nu \\ \lambda=even \\ \mu=odd}} a_{3\lambda\mu\nu}\bar{P}_\lambda(X)\bar{P}_\mu(Y)\bar{P}_\nu(Z)e_3\Bigg).\end{aligned} \tag{18}$$

Again, all terms are still present in the expansion in (17); we have simply chosen to write them in a particular order. It is now possible to factor $\boldsymbol{\Gamma}$ into 16 blocks with only the four blocks along the diagonal having non-zero values, because u^{ss} terms only couple to other u^{ss} terms, etc. Similar considerations show that three mirror planes perpendicular to the x, y, and z axes lead to $\boldsymbol{\Gamma}$ being factored into 64 blocks with eight non-zero blocks along the diagonal. If two mirror planes are used, four eigenvalue problems would be solved and the results combined. Likewise three mirror planes lead to a total of eight individual problems to solve. Despite the overhead of dealing with several problems, it will be demonstrated below that the net computational savings are tremendous.

Mirror planes are convenient in that only a single coordinate changes sign under this type of symmetry operation. Other types of symmetry can also be exploited, although the restrictions they impose on the displacement may be more complicated. As discussed above, the generic procedure is to write the expansion of the displacement in terms of symmetric and antisymmetric modes and calculate individual eigenvalue problems for each mode.

As an example of another symmetry operation, we consider samples which possess a twofold rotation axis about x. In this case, both the y and z coordinates change sign, resulting in simultaneous restrictions on μ and ν. Proceeding similarly to the arguments above, a symmetric displacement function requires that u_x should not change sign while both u_y and u_z will change sign under the symmetry operation. These conditions are met by requiring $\mu+\nu$ be even for u_x and odd for u_y and u_z. The opposite conditions apply for the antisymmetric modes. The grouping of the displacement functions for such a twofold rotation about the x axis is

$$\boldsymbol{u}^{s}(\boldsymbol{r}) = \frac{1}{\sqrt{L_1L_2L_3}}\Bigg(\sum_{\substack{\lambda\mu\nu \\ \mu+\nu=even}} a_{1\lambda\mu\nu}\bar{P}_\lambda(X)\bar{P}_\mu(Y)\bar{P}_\nu(Z)e_1$$

$$+\sum_{\substack{\lambda\mu\nu\\ \mu+\nu=odd}} a_{2\lambda\mu\nu}\bar{P}_\lambda(X)\bar{P}_\mu(Y)\bar{P}_\nu(Z)e_2+\sum_{\substack{\lambda\mu\nu\\ \mu+\nu=odd}} a_{3\lambda\mu\nu}\bar{P}_\lambda(X)\bar{P}_\mu(Y)\bar{P}_\nu(Z)e_3\Bigg)$$

$$\boldsymbol{u}^a(\boldsymbol{r})=\frac{1}{\sqrt{L_1L_2L_3}}\Bigg(\sum_{\substack{\lambda\mu\nu\\ \mu+\nu=odd}} a_{1\lambda\mu\nu}\bar{P}_\lambda(X)\bar{P}_\mu(Y)\bar{P}_\nu(Z)e_1$$

$$+\sum_{\substack{\lambda\mu\nu\\ \mu+\nu=even}} a_{2\lambda\mu\nu}\bar{P}_\lambda(X)\bar{P}_\mu(Y)\bar{P}_\nu(Z)e_2+\sum_{\substack{\lambda\mu\nu\\ \mu+\nu=even}} a_{3\lambda\mu\nu}\bar{P}_\lambda(X)\bar{P}_\mu(Y)\bar{P}_\nu(Z)e_3\Bigg). \tag{19}$$

As was the case above, matrix elements involving u^s and u^a will be zero, so that the matrices may be broken into two non-zero blocks along the diagonal, and two smaller eigenvalue problems result. Guided by (19) the first matrix is calculated using only combinations of (λ, μ, ν) from the symmetric portion of the expansion and the eigenvalues and eigenvectors determined. The process is then repeated using the combinations of (λ, μ, ν) from the antisymmetric portion of the expansion and a second set of eigenvalues and eigenvectors obtained. The two sets of eigenvalues and eigenvectors can then be combined and sorted in ascending order of eigenvalues.

The displacement for a sample with inversion symmetry can be written as a sum of symmetric terms and a sum of antisymmetric terms, with a restriction on $\lambda+\mu+\nu =$ (odd or even). Grouping the expansion in this manner will result in two non-zero blocks. Inversion symmetry is important because any elastic constant matrix has this symmetry. Tables 1–3 list the restrictions placed on various combinations of λ, μ, and ν for the two types of mode for various symmetry operations.

Table 1. Classification of the parity of the displacement function for a mirror plane parallel to the yz, xz, or xy plane. The conditions on the integers λ, μ, and ν are given.

	Symmetric			Antisymmetric		
	yz	xz	xy	yz	xz	xy
	λ	μ	ν	λ	μ	ν
u_x	odd	even	even	even	odd	odd
u_y	even	odd	even	odd	even	odd
u_z	even	even	odd	odd	odd	even

Table 2. Classification of the parity of the displacement functions for twofold rotations about the x, y, or z axis. The conditions on the integers λ, μ, and ν are given.

	Symmetric			Antisymmetric		
	x	y	z	x	y	z
	$\mu+\nu$	$\lambda+\nu$	$\lambda+\mu$	$\mu+\nu$	$\lambda+\nu$	$\lambda+\mu$
u_x	even	odd	odd	odd	even	even
u_y	odd	even	odd	even	odd	even
u_z	odd	odd	even	even	even	odd

The symmetry arguments have been discussed for the specific case of Legendre polynomials as basis functions, but the essential feature is the parity of the basis functions.

Table 3. Classification of the parity of the displacement functions for an inversion operation. The conditions on the integers λ, μ, and ν are given.

	Symmetric $\lambda+\mu+\nu$	Antisymmetric $\lambda+\mu+\nu$
u_x	odd	even
u_y	odd	even
u_z	odd	even

Table 4. Computation times, using zero, one, etc mirror planes, for one full iteration for a rectangular parallelepiped with hexagonal crystallographic symmetry. The computations were performed on a Hewlett–Packard 735 workstation.

No of mirror planes	No of matrices	Computation time (min:s)
0	1	11:10
1	2	4:27
2	4	1:53
3	8	0:35

Thus, the arguments are the same if $x^\lambda y^\mu z^\nu$ are chosen as the basis functions [24]. The matrices factor in exactly the same way. The advantage of using symmetry is illustrated in table 4. A workstation (Hewlett–Packard 735) was used to compute the eigenvalues for a rectangular parallelepiped having hexagonal crystalline symmetry. Listed in table 4 are the computation times for one iteration, i.e. one computation of the eigenvalues and a correction to the input elastic constants (discussed below). The computations were carried out using no mirror plane, one mirror plane, etc. Mirror planes were convenient for generating the table; however, other types of symmetry result in similar performance.

The time quoted in table 4 is the time needed to solve the entire set of matrices. As can be seen in the table, the use of symmetry greatly speeds the calculations. If a sample has even a single mirror plane, the computation time is reduced by 60%. This becomes even more important since 20–40 iterations may be needed, depending on the accuracy of the initial estimates for the parameters. As can be seen in the table, a 20-fold decrease in the computational time can be achieved if the sample has sufficiently high symmetry.

It was stated earlier that if both the sample shape and elastic constant matrix have symmetry elements in common it is possible for the matrix to be factored. Now, we will explore why the symmetric and antisymmetric modes are uncoupled. As an example we consider explicitly a sample with a single yz mirror plane in both the sample shape and in the elastic constant matrix. The elements of $\mathbf{\Gamma}$ are calculated as given in (12) and the parities of the components of the displacement for a yz mirror plane are given in table 1. Notice that each element of $\mathbf{\Gamma}$ is the sum of nine individual terms, each of which is an elastic constant multiplied by an integral. There are two separate reasons why terms from the different mode types are uncoupled: the corresponding elastic constant matrix may be zero; the integral may vanish.

First, consider the effect of a symmetry operation on an elastic constant. Federov [6] shows that the effect of symmetry operations in which one coordinate transforms to another, including possible sign changes, is to exchange values of 1, 2, 3 in the subscript for the elastic constant with the transformed values. It is important to use the four-index form of the elastic constant matrix when doing this. In addition, the new elastic constant is multiplied

by $(-1)^n$ where n is the number of sign changes due to the transformation. For example, consider the effect of a yz mirror plane on C_{1222}. In this case, because the only effect of the transformation is to replace '1' with '-1', we obtain $C_{1222} = -C_{1222}$. Thus $C_{1222} = 0$ for any material which has a yz mirror plane. Keeping this in mind, we are now ready to examine the reasons that $\mathbf{\Gamma}$ can be factored into blocks. In the following, we consider an element of $\mathbf{\Gamma}$ using one term from the symmetric part of the expansion for the displacement and one term from the antisymmetric part.

Case 1: $i = i' = 1$; u_x^s, u_x^a. From the preceding paragraph, we know that the effect of a yz mirror plane on the elastic constant matrix is that all elastic constants in which the number '1' appears in the subscripts an odd number of times will be identically equal to zero. Thus of the nine terms for a given element of $\mathbf{\Gamma}$ with $i = i' = 1$, terms with the combinations of $(j, j') = \{(1, 2), (1, 3), (2, 1), (3, 1)\}$ will be identically equal to zero because the elastic constant involved will be zero. So in this case, only five of the nine terms remain to be examined. Next consider the term with $(j, j') = (1, 1)$ and recall that the parity of u_x^s is odd with respect to x and the parity of u_x^a is even. This term will be zero because we will then be integrating the derivative of an odd function of x, $\partial u_x^s/\partial x$, multiplied by the derivative of an even function of x, $\partial u_x^a/\partial x$, over a macroscopic sample with a yz mirror plane. The remaining four terms all involve derivatives with respect to y or z, not x, so in these cases the integral over x will be an integral of an odd function of x multiplied by an even function of x, so all four of these terms will be zero. It was stated earlier that the sample and crystal structure must have symmetry elements in common to obtain a decoupling of the matrix. We now see that certain terms vanish because the corresponding elastic constant is zero. Other terms vanish because the integrand is an odd function over the range of integration.

Case 2: $i = 1$, $i' \neq 1$; u_x^s, $u_{(y\ or\ z)}^a$. In this case, the only elastic constants that will not vanish are those with $(j, j') = (1, 2), (1, 3), (2, 1), (3, 1)$. All other elastic constants for these elements of Γ will be zero since all other combinations contain an odd number of 1s. We only need to examine the remaining four cases. For the first two cases, $(j, j') = (1, 2), (1, 3)$, recall u_x^s has odd parity with respect to x and u_y^a and u_z^a also have odd parity with respect to x. These two terms involve an integral over x of a derivative with respect to x of an odd function of x, multiplied by an odd function of x, and will vanish. Finally, the remaining two terms, $(j, j') = (2, 1), (3, 1)$ will involve an integral over x of an odd function of x multiplied by the derivative with respect to x of an odd function of x, again vanishing.

Case 3: $i \neq 1$, $i' = 1$; $u_{(y\ or\ z)}^s$, u_x^a. The argument proceeds the same as for case 2 except that even functions are involved.

Case 4: $i \neq 1$, $i' \neq 1$; $u_{(y\ or\ z)}^s$, $u_{(y\ or\ z)}^a$. Once again, consideration of the non-zero elastic constants leaves only the terms with $(j, j') = (1, 1), (2, 2), (2, 3), (3, 2), (3, 3)$ to be considered. Equation (16) shows that $u_{(y\ or\ z)}^s$ has even parity with respect to x and $u_{(y\ or\ z)}^a$ has odd parity. The first set of $(j, j') = (1, 1)$ to be examined will involve an x integration of the derivative of an even function multiplied by the derivative of an odd function, which vanishes. The remaining terms will all involve an x integration of an even function multiplied by an odd function, which also vanishes.

In each case above, any term from the symmetric portion of the expansion for the displacement combined with any term from the antisymmetric portion of the expansion will vanish because either the corresponding elastic constant is zero, or the integral is zero. An inversion operation imposes no restrictions on the elastic constants; all terms between symmetric and antisymmetric modes vanish for a sample with inversion symmetry because

the integrals are zero. Depending on the basis functions chosen, it may be necessary to factor **E** as well as **Γ**. It is easy to show that the groupings discussed above also factor **E**.

4.2. Determination of the sample parameters

4.2.1. Minimization of the error function. The ability to calculate the resonant frequencies, given the parameters for a particular sample, is but the first part of the calculations in RUS. It is usually the case that one is interested in the inverse problem, the determination of some of the parameters from the measured frequencies. Most often the elastic constants are of interest but other parameters, such as the exact sample dimensions or perhaps the orientation of the crystal with respect to the sample axes, may also be desired. An effective method for determining the parameters for a given sample has been developed [4]. Given a set of elastic constants and information about the sample, it is possible to calculate a set of resonant frequencies as described earlier. This set of calculated frequencies is then compared to the set of measured frequencies. A measure of the closeness of the fit can be described in terms of some function, such as

$$\chi = \sum_n w_n \frac{(f_n - g_n)^2}{g_n^2} \tag{20}$$

where w_n is the weight to give the normalized difference between the calculated frequencies f_n and the measured frequencies g_n. It is assumed that the function given in (20) will have a minimum when the *correct* set of parameters is achieved. If the current set of parameters $p_{\alpha 0}$ is sufficiently close to the correct set of parameters p_α, an expansion of (20) to second order will provide a close approximation to the function χ.

$$\chi(\boldsymbol{p}) = \chi(\boldsymbol{p}_0) + (\partial\chi/\partial p_\alpha)_{p_{\alpha 0}}(p_\alpha - p_{\alpha 0}) + \frac{1}{2}(\partial^2\chi/(\partial p_\alpha \partial p_\beta))_{p_{\alpha 0} p_{\beta 0}}(p_\alpha - p_{\alpha 0})(p_\beta - p_{\beta 0}) + \cdots. \tag{21}$$

The repeated indices, α and β, are to be summed over the number of parameters, M, which are to be varied. Since χ will have a minimum when $\boldsymbol{p}$ is the correct set of parameters, the derivative of (21) with respect to each of the parameters, p_α, will equal zero. Hence, we arrive at a set of M equations

$$(\partial\chi/\partial p_\alpha)_{p_{\alpha 0}} + (\partial^2\chi/(\partial p_\alpha \partial p_\beta))_{p_{\alpha 0} p_{\beta 0}}(p_\beta - p_{\beta 0}) = 0. \tag{22}$$

Solving for p_α provides

$$p_\alpha = p_{\alpha 0} - \mathbf{A}^{-1}_{\alpha\beta}\mathbf{B}_\beta \tag{23}$$

where the derivatives appearing in (22) are the elements of the matrices **A** and **B** in (23). Equation (23) then provides a means of calculating a new set of parameters, based on the current parameters, which gives a better fit between the measured and calculated frequencies. These new parameters are used in (9) and the problem is solved iteratively. It only remains to calculate the first and second derivatives appearing in (22). This is easily done as follows, and also provides a measure of the dependence of each mode on each parameter.

4.2.2. Calculation of the derivatives of the error function. The derivatives needed for (22) and (23) are easily obtained from (9) and (20). Differentiating (20) gives

$$\frac{\partial\chi}{\partial p_\alpha} = 2\sum_n w_n \frac{(f_n - g_n)}{g_n^2}\frac{\partial f_n}{\partial p_\alpha} \tag{24}$$

and

$$\frac{\partial^2 \chi}{\partial p_\alpha \partial p_\beta} = 2\sum_n \frac{w_n}{g_n^2}\frac{\partial f_n}{\partial p_\alpha}\frac{\partial f_n}{\partial p_\beta} + 2\sum_n w_n \frac{(f_n - g_n)}{g_n^2}\frac{\partial^2 f_n}{\partial p_\alpha \partial p_\beta}. \tag{25}$$

The second term on the right-hand side of (25) may be dropped without affecting the final results [4, 26]; thus, we need only the first derivatives of f_n with respect to each of the parameters in order to solve for p_β in (23). These derivatives are derived from (9) as shown below.

The parameters p_α are usually the elastic constants, but it is frequently convenient to allow the sample dimensions to vary somewhat as well. In this case one needs derivatives of f_n with respect to the sample dimensions as well as the elastic constants. Since both $\mathbf{\Gamma}$ and the density, ρ, appearing in (9) are functions of the sample dimensions, the computation of the derivatives is simplified by introducing a new matrix $\mathbf{\Gamma}^* = (\text{volume})\mathbf{\Gamma}$. The eigenvalue equation then becomes

$$\mathbf{\Gamma}^* \boldsymbol{a} = m\omega^2 \mathbf{E}\boldsymbol{a} \tag{26}$$

where m, the sample mass, is constant. Realizing that the resonant frequencies ω, the matrices $\mathbf{\Gamma}^*$ and $\mathbf{E}$, and the eigenvectors $\boldsymbol{a}$ are all functions of the sample parameters allows the derivative of (26) to be written

$$\frac{\partial \mathbf{\Gamma}^*}{\partial p_\alpha}\boldsymbol{a} + \mathbf{\Gamma}^*\frac{\partial \boldsymbol{a}}{\partial p_\alpha} = m\frac{\partial \omega^2}{\partial p_\alpha}\mathbf{E}\boldsymbol{a} + m\omega^2\frac{\partial \mathbf{E}}{\partial p_\alpha}\boldsymbol{a} + m\omega^2\mathbf{E}\frac{\partial \boldsymbol{a}}{\partial p_\alpha}. \tag{27}$$

Now multiplying from the left by $\boldsymbol{a}^T$ and taking the transpose of the entire equation, remembering that $\mathbf{\Gamma}^*$ and $\mathbf{E}$ are both real, symmetric matrices gives

$$\boldsymbol{a}^T\frac{\partial \mathbf{\Gamma}^*}{\partial p_\alpha}\boldsymbol{a} + \frac{\partial \boldsymbol{a}^T}{\partial p_\alpha}\mathbf{\Gamma}^*\boldsymbol{a} = m\frac{\partial \omega^2}{\partial p_\alpha}\boldsymbol{a}^T\mathbf{E}\boldsymbol{a} + m\omega^2\boldsymbol{a}^T\frac{\partial \mathbf{E}}{\partial p_\alpha}\boldsymbol{a} + m\omega^2\frac{\partial \boldsymbol{a}^T}{\partial p_\alpha}\mathbf{E}\boldsymbol{a}. \tag{28}$$

The second and fifth terms are nothing more than (26) multiplied from the left by $\partial \boldsymbol{a}^T/\partial p_\alpha$, which cancel. The needed derivatives are

$$\frac{\partial f_n}{\partial p_\alpha} = \frac{1}{(8\pi^2 f_n)}\frac{\partial \omega_n^2}{\partial p_\alpha} = \frac{1}{8\pi^2 f_n(m\boldsymbol{a}_n^T\mathbf{E}\boldsymbol{a}_n)}\boldsymbol{a}_n^T\left(\frac{\partial \mathbf{\Gamma}^*}{\partial p_\alpha} - m\omega_n^2\frac{\partial \mathbf{E}}{\partial p_\alpha}\right)\boldsymbol{a}_n. \tag{29}$$

Once again, the problem is reduced considerably if $\mathbf{E}$ is the identity matrix. In addition, many FORTRAN libraries (Eispack, Lapack, etc) return the eigenvectors of a matrix already normalized, which further simplifies the calculation.

Thus, determining the improved set of parameters for a given sample consists of solving (23), using the derivatives from (29). This procedure works well if the initial set of parameters is reasonably close to the correct ones. If this is not the case, the usual procedure is simply to move opposite to the gradient. Thus, (23) is replaced by

$$p_\alpha = p_{\alpha 0} - \text{constant}(B_\alpha). \tag{30}$$

Proper choices of the constant and elegant ways of combining (23) and (30) have been discussed [4, 26].

One of the more troubling problems is in recognizing missing resonances in the list of measured frequencies. It has been found helpful to begin by fitting only the first five to ten resonances initially and varying the elastic constants manually. Missing resonances are then often identified by a large *change* in the percentage error at the missing mode. The usual procedure is to insert a mode with zero frequency at that position in the list and use the weight $w_n = 0$ in (24) and (25) to ignore that term. It is often the case that a detailed experimental search near the calculated frequency will then find the missing mode. It is also

useful in many cases to remount the sample while searching for missing modes. Figure 3 shows an example in which the mode at 788 kHz was not seen on the initial scan, but was observed after remounting the sample. This effect is understood when it is realized that only the motion of the corner of the parallelepiped *perpendicular* to the transducer surface generates a signal. If a mode accidentally has corner motion *parallel* to the transducer surface, it will not be observed. Remounting of the sample will usually be at a somewhat different angle and result in a component of the motion perpendicular to the transducer surface.

4.3. Effects of dissipation

The use of RUS to measure ultrasonic attenuation is less well advanced than the use of the technique for modulus measurements. This is unfortunate because conventional attenuation measurements have been shown to be sensitive to a wide range of interactions. The high Q values of many resonance lines will enhance sensitivity. High Q values in conventional ultrasonic standing wave measurements have provided enough sensitivity to detect ultrasonically excited electron spin resonance [27] and nuclear magnetic resonance [28], which are extremely small effects. Motion with a rate comparable to the ultrasonic frequency leads to relaxational attenuation. Thus, RUS should be a sensitive tool for the study of motion in the megahertz and lower range. This time scale is difficult to investigate with techniques such as neutron scattering.

Most resonant frequencies in RUS depend on a combination of elastic constants. This dependence complicates the interpretation of the results. The effect of the attenuation may be expressed in terms of a complex elastic constant and a complex frequency. In many cases the complex part is much smaller than the real part. In such cases the loss associated with a particular resonance line can be expressed in terms of the loss attributed to each elastic constant [29, 30]. An oscillator with damping can be represented by a complex frequency $\tilde{f} = f_0 + \mathrm{i}f^*$. It is easy to show that the Q characterizing the resonant response of the oscillator to an external force is related to $\tilde{f}$ by

$$1/Q = 2f^*/f_0 \tag{31}$$

if $f^*/f_0 \ll 1$. Here, as usual, $Q = f_0/\Delta f$ where Δf is measured between the half-power points of the resonance. The elastic Lagrangian may be separated into spatial and temporal parts [21], where the temporal part may be represented by $\exp(\mathrm{i}2\pi f t)$. Replacing f by $\tilde{f}$ in this expression relates the attenuation to f^*. The *amplitude* attenuation coefficient often measured in pulse-echo experiments, α, is related to Q by $\alpha = \pi f Q^{-1}$ if α is measured in units of inverse time. Q^{-1} is usually called the internal friction. Denoting Q_k^{-1} as the internal friction associated with eigenmode k and Q_{mn}^{-1} as the internal friction associated with the elastic constant C_{mn}, it has been shown [29] that

$$\frac{1}{Q_k} = \frac{2}{f_k}\sum_{mn}\frac{\partial f_k}{\partial C_{mn}}\frac{C_{mn}}{Q_{mn}} = 2\sum_{mn}\frac{\partial(\log f_k)}{\partial(\log C_{mn})}\frac{1}{Q_{mn}}. \tag{32}$$

This formula is derived under the assumption that the internal friction is independent of frequency, which may not always be true, but may be a reasonable approximation if the frequency range is not too wide. As discussed above, the derivatives are usually calculated as part of the inverse problem to find the elastic constants. Thus, by measuring a relatively large number of the Q_k^{-1} it is in principle possible to find the small number of independent Q_{mn}^{-1} by a least-squares method. The technique has been applied to measure the internal friction in MgO [29, 30]. This method is potentially very powerful. The complete determination

of all the Q_{mn}^{-1} would be extremely valuable. However, it seems that the determination of the Q_{mn}^{-1} is not yet very accurate, perhaps because of mode-dependent extrinsic losses. The measured Q_k^{-1} reflect all the energy dissipation from the resonance, either intrinsic or extrinsic while the Q_{mn}^{-1} refer only to intrinsic losses.

5. Applications of RUS

5.1. Phase transitions

RUS is especially useful for the study of phase transitions. The ability to use much smaller samples means that inhomogeneities are less of a problem. The absence of a bond between the sample and transducer offers the possibility of making measurements on systems undergoing considerable thermal contraction at the transition. The description of phase transitions often starts from an expression for the free energy of the system [31–33]

$$F = F_0(T) + F_L(\eta_i) + F_e(e_j) + F_c(\eta_i, e_j) \tag{33}$$

where η_i represents one or more order parameters which describe the transition and e_j are the elastic strains. $F_e(e_j)$ is just the elastic energy

$$F_e = \frac{1}{2}\sum_{i,j} C_{ij} e_i e_j. \tag{34}$$

(We replace the four-index tensor notation for the elastic constants by the two-index matrix notation [5], with a similar change for the strains.) F_L, the Landau free energy, is usually represented by a polynomial in powers of η_i. F_c represents a coupling between the strain and the order parameter. It is this coupling which leads to effects on the elastic constants near the phase transition. F_0 represents other contributions to the free energy which do not involve η or e. The equilibrium states of the system are found by minimizing F with respect to the η_i and e_j. The elastic constants are the second derivatives of F with respect to strain,

$$C_{ij} = \partial^2 F/(\partial e_i \partial e_j). \tag{35}$$

The purely elastic contribution to the elastic constants corresponds to calculating C_{ij} with $\eta_i = 0$. The effects of the phase transition are found by assuming that the η_i respond to the ultrasonic strains such that $\partial F/\partial \eta_i = 0$ at all times. The result for the elastic constants is [34, 35, 25]

$$C_{mn} = C_{mn}^0 + \frac{\partial^2 F_c}{\partial e_m \partial e_n} - \sum_{k,l}\left[\frac{\partial^2 F}{\partial e_m \partial \eta_k}\right]\left[\frac{\partial^2 F}{\partial \eta_k \partial \eta_l}\right]^{-1}\left[\frac{\partial^2 F_c}{\partial e_n \partial \eta_l}\right] \tag{36}$$

where C_{mn}^0 are the elastic constants excluding the effects of the phase transition, while the remaining terms are due to the phase transition. A great restriction on the possible forms of C_{mn} is possible by requiring that F be invariant under the symmetry operations of the crystal. F_e will automatically satisfy this requirement by using the appropriate elastic constant matrix for the crystal. F_L can easily be constructed to satisfy this requirement [32]. Various forms of F_c can satisfy the symmetry requirements; however, the different forms predict different experimental results. A comparison of experimental and theoretical results gives information about F_c and thus sheds light on the nature of the phase transition. Such an approach has been used [36] on superconducting $La_{1.86}Sr_{0.14}O_4$. The study of the strong temperature dependence of the tetragonal elastic constants above the tetragonal to orthorhombic structural phase transition in $La_{2-x}Sr_xO_4$ has raised important questions

about the nature of this second-order transition. RUS can be useful for a quick qualitative measurement of elastic properties to see whether further work is warranted. In one case [37] strong temperature-dependent softening of a resonant frequency in an unoriented chip of $La_{1.82}Sr_{0.18}O_4$ indicated that the softening observed on oriented crystals at lower values of x was universal. The volume of the chip was only about 0.06 mm^3.

We now consider in some detail a first-order phase transition in $LiKSO_4$. This material is one of a large number of sulphate compounds of the form $ABSO_4$ (A, B = Li, Na, K, Cs, Rb, Ag, H, and NH_4). These materials exhibit a rich variety of phase transitions due largely to the motion of the SO_4 tetrahedra. At high temperatures the tetrahedra undergo rapid rotation resulting in a relatively high-symmetry phase. As the temperature is lowered the rapid rotation freezes out and various tilts of the tetrahedra give rise to a series of phase transitions. The room-temperature structure of $LiKSO_4$ is hexagonal ($P6_3$). At approximately 210 K on cooling the material transforms to a trigonal phase ($P31c$). The material returns to the hexagonal phase at approximately 240 K on warming. Remarkably, the crystal shows no visible cracks or damage due to this first-order phase transition. We made RUS measurements [38] on a single-crystal parallelepiped of room-temperature dimensions $1.349 \times 1.528 \times 1.361$ mm^3. We identified 38 of the first 40 resonances at room temperature and fitted the measured frequencies to a hexagonal elastic constant matrix with a typical rms error of 0.16%. The measured frequencies shifted strongly on entering the trigonal phase, and the results could no longer be fitted by the hexagonal elastic constant matrix, consistent with the assignment of this phase to the trigonal class.

The most general trigonal case requires seven independent elastic constants. However, a crystal such as $LiKSO_4$ with a glide plane parallel to the c axis requires only six. If the axis system is chosen such that the glide plane is perpendicular to the x axis the elastic constant matrix is given by

$$\mathbf{C} = \begin{pmatrix} C_{11} & C_{12} & C_{13} & C_{14} & 0 & 0 \\ C_{12} & C_{11} & C_{13} & -C_{14} & 0 & 0 \\ C_{13} & C_{13} & C_{33} & 0 & 0 & 0 \\ C_{14} & -C_{14} & 0 & C_{44} & 0 & 0 \\ 0 & 0 & 0 & 0 & C_{44} & C_{14} \\ 0 & 0 & 0 & 0 & C_{14} & C_{66} \end{pmatrix} \tag{37}$$

with $C_{66} = \frac{1}{2}(C_{11} - C_{12})$. Setting $C_{14} = 0$ gives the hexagonal elastic constant matrix. In general the elastic constant matrix may possess higher symmetry than the crystal because operations such as inversions and pure translations have no effect on $\mathbf{C}$. Thus, the trigonal elastic constant matrix is invariant under a reflection in the yz plane, while the crystal only has a yz glide plane. Not only is the trigonal elastic constant matrix invariant under a reflection in the yz plane, but it also is invariant under a twofold rotation about the x axis. These two symmetries were used to split the eigenvalue problem into four smaller problems as discussed in subsubsection 4.1.2 [25].

The measured frequencies in the trigonal phase were fitted to the trigonal elastic constant matrix to a typical rms accuracy of 0.35%. The reason for the decreased accuracy in the trigonal phase could be some misalignment of the trigonal crystalline axes with the parallelepiped axes. Any such misalignment is less important in the hexagonal phase because the hexagonal system has the unusual property that it is elastically isotropic in the basal plane. The temperature dependence of the elastic constants is shown in figure 6. The symbols represent the data while the solid lines represent a fit to the data to be described below. The most significant feature is the large change in the elastic constants at the trigonal–hexagonal phase boundary, and the large hysteresis. The results for C_{14} merit

special attention. An attempt was made to fit the data in the trigonal phase with $C_{14} = 0$, i.e. with a hexagonal elastic constant matrix, but it was not possible to obtain a satisfactory fit. Also, one attempt was made to fit the room-temperature data with a non-zero value of C_{14}. The initial values for the elastic constants in the calculation were the values obtained with the hexagonal matrix along with $C_{14} = 0.014 \times 10^{11}$ Pa. Within a few iterations the program drove the value of C_{14} down to 0.003×10^{11} Pa. The zero values of C_{14} in figure 6 simply mean that the frequencies measured in the hexagonal phase were fitted with the hexagonal phase elastic constant matrix.

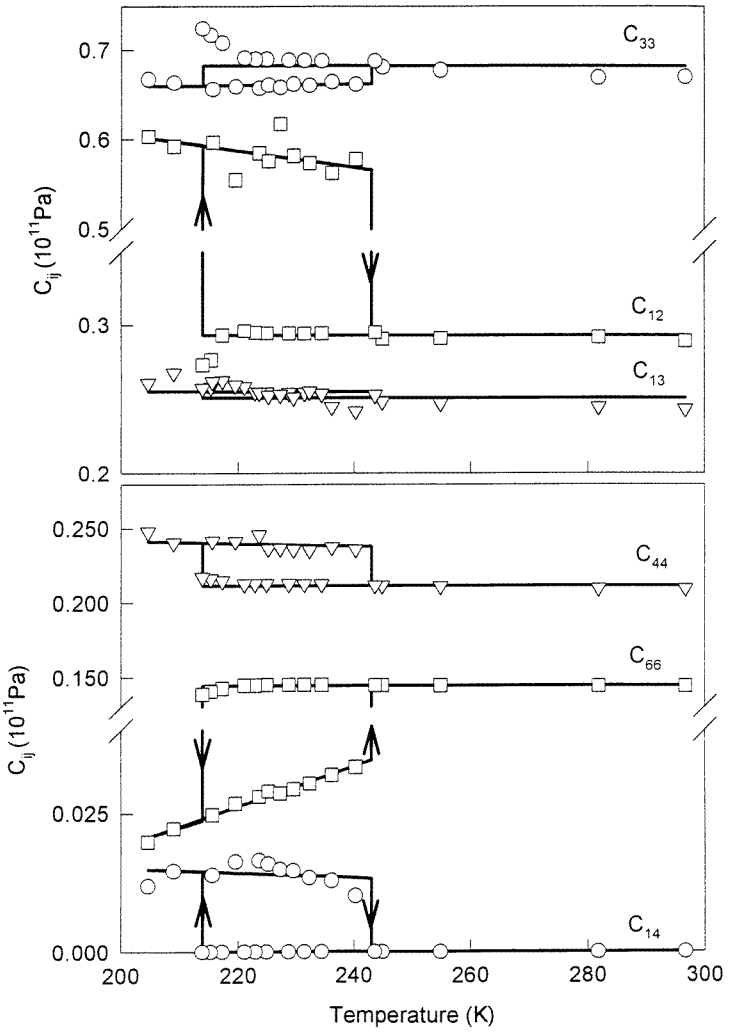

Figure 6. The temperature dependence of elastic constants for $LiKSO_4$. The arrows indicate observed discontinuities in the measurements. Note the broken scale for the C_{ij}.

The phase transitions in $LiKSO_4$ involve tilts of the SO_4 tetrahedra. There are two tetrahedra per unit cell and it turns out [38] that the hexagonal and trigonal phases can be described by two order parameters, η_1 and η_2, which describe the configurations

corresponding to the two crystalline symmetries. The hexagonal phase corresponds to $(\eta_1, \eta_2) = (\pm x, 0)$ while the trigonal phase corresponds to $(\eta_1, \eta_2) = (0, \pm y)$. Imry [39] has developed the Landau theory for a system with two coupled order parameters. We follow his treatment and set

$$F_L(\eta_1, \eta_2) = a_1\eta_1^2 + \tfrac{1}{2}b_1\eta_1^4 + a_2\eta_2^2 + \tfrac{1}{2}b_2\eta_2^4 + \lambda\eta_1^2\eta_2^2 \tag{38}$$

where a_i and b_i are the usual Landau expansion coefficients and λ describes the strength of coupling between η_1 and η_2. Imry shows that this expression describes a first-order transition if $\lambda > (b_1b_2)^{1/2}$, which we take to be the case here. We use the RUS results to determine the nature of $F_c(\eta_1, \eta_2, e_i)$. As mentioned above, the free energy must be invariant under the symmetry operations of the crystal. The order parameters which we have defined are scalars, thus $F_L(\eta_1, \eta_2)$ is automatically invariant. Changing the sign of either of the η parameters does not change the symmetry of the crystal, thus the free energy must be invariant under such sign changes. We first try the simplest form of $F_c(\eta_1, \eta_2, e_i)$ compatible with these considerations, coupling quadratic in the order parameters and linear in the strains. We require the form to be invariant under the operations of $P31c$, which gives

$$F_{1c}(\eta_1, \eta_2, e_i) = (k_{11}\eta_1^2 + k_{21}\eta_2^2)(e_1 + e_2) + (k_{13}\eta_1^2 + k_{23}\eta_2^2)e_3 \tag{39}$$

where the k are coupling coefficients. This form is also invariant under the operations of $P6_3$. Using (36) and (39), the predicted changes in the elastic constants at the phase transitions are

$$\begin{aligned} &\Delta C_{12} \neq 0 \qquad \Delta C_{13} \neq 0 \qquad \Delta C_{33} \neq 0 \\ &\Delta C_{14} = \Delta C_{44} = \Delta C_{66} = 0. \end{aligned} \tag{40}$$

Clearly these predictions are in strong disagreement with the results of figure 6.

Next, we try bi-quadratic coupling in the order parameters and strain. We take

$$F_{2c} = \frac{1}{2}\eta_1^2 \sum_{i,j} k_{1ij}e_ie_j + \frac{1}{2}\eta_2^2 \sum_{i,j} k_{2ij}e_ie_j \tag{41}$$

where k_{1ij} and k_{2ij} are the bi-quadratic coupling coefficients. Because F_{2c} is of the same form as the elastic energy, it will be invariant under the symmetry operations of the crystal if the matrices k_{1ij} and k_{2ij} have the same form as the elastic constant matrices in each phase. The elastic constants are easily calculated to be

$$C_{mn}^{hex} = C_{mn} + k_{1mn}\eta_1^2 \qquad C_{mn}^{trig} = C_{mn} + k_{2mn}\eta_2^2 \tag{42}$$

where the η parameters appearing in (42) are the equilibrium values of the order parameters in each phase. Considering the form of the k coefficients just mentioned, it is seen that bi-quadratic coupling between the order parameters and strain permits changes in all the elastic constants at the transition, in agreement with the experimental results. The results give information about the relative magnitudes and signs of the k coefficients which could be used to place constraints on any microscopic theory. The temperature dependence of the elastic constants is related to the temperature dependence of the equilibrium values of η_1 and η_2. Using the usual Landau approach to calculate the η parameters gives the solid lines of figure 6. The Imry approach does allow for hysteresis, but we do not have enough information to calculate the transition temperatures. The arrows in figure 6 simply indicate the observed transitions.

5.2. Hydrogen–metal systems

RUS has been used to study metals containing large amounts of hydrogen. Many of the transition and rare-earth metals readily absorb hydrogen, which occupies interstitial sites in the host lattice. The hydrogen mobility can be rather high even at liquid helium temperatures. There are effects on the elastic constants and on the internal friction (dissipation). The absorption of hydrogen is almost always associated with an expansion of the lattice. Thus, one may reasonably expect an effect on the elastic constants and this is indeed found to be the case [40]. In addition, accurate RUS measurements [41] on the Laves-phase pseudo-binary compounds $Zr(Al_xFe_{1-x})_2$ demonstrated a correlation of the hydrogen capacity with the bulk and shear modulus for $0.04 \leqslant x \leqslant 1$.

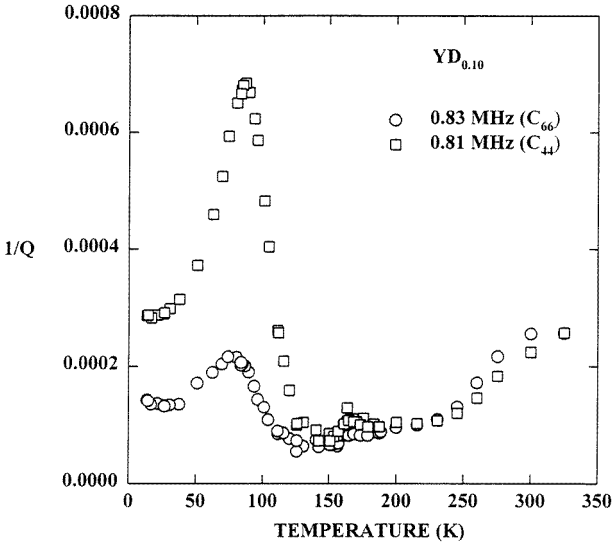

Figure 7. Q^{-1} against temperature for a single-crystal $YD_{0.10}$ parallelepiped. The mode at 0.81 MHz depends almost entirely on C_{44} while the mode at 0.83 MHz depends almost entirely on C_{66}.

The dynamical aspects of hydrogen in metals are reflected in the dissipation [42–44]. An example is shown in figure 7 for measurements on a parallelepiped of yttrium containing deuterium. There is a prominent loss peak at approximately 90 K. It was determined by a comparison of computed and measured frequencies that the peak at 0.81 MHz depends almost entirely on the elastic constant C_{44} while the one at 0.83 MHz depends almost entirely on C_{66}. Thus, the results demonstrate a strong mode dependence for the loss. The diffusive motion of hydrogen in metals is generally understood to be due to the hopping or tunnelling of hydrogen between interstitial sites. Considering a simple model where the hydrogen can occupy two different sites differing in energy by $2E$ and can move between those sites with a relaxation time τ, the internal friction $1/Q_{ij}$ corresponding to the elastic constant C_{ij} is given by a relaxation-type expression [45–46]

$$1/Q_{ij} = (n_0/C_{ij}k_BT)[\partial E/\partial e_i][\partial E/\partial e_j]\mathrm{sech}^2[E/k_BT]\omega\tau/(1+\omega^2\tau^2) \quad (43)$$

where n_0 is the concentration of hydrogen participating in the relaxation, k_B is Boltzmann's constant, and ω is the angular frequency of the ultrasonic vibration. It can be seen

immediately from figure 7 that $(\partial E/\partial e_4)^2 \simeq 4(\partial E/\partial e_6)^2$. Such a strong mode dependence gives insight into the sites involved in the hydrogen motion.

The relaxation time is usually strongly dependent on temperature. In the case of a single relaxation time τ and $E \ll k_B T$, (43) gives a simple attenuation peak with the maximum occurring when $\omega\tau \simeq 1$. It is tempting to interpret the peaks of figure 7 in this way. However, the case of hydrogen in metals, especially at low temperatures, is not so simple and the data of figure 7 cannot be fitted so simply [42]. The situation with hydrogen in scandium [43] differs even farther from the simple, classical expression. There appear to be distributions of τ and E. Further, it seems clear that tunnelling is involved and the interaction of the tunnelling system with conduction electrons and thermal phonons changes the picture in a fundamental way [47]. The picture is not yet clear, and research in this area continues.

5.3. Other uses

Some of the unique capabilities of RUS were demonstrated in a remarkable experiment on quasicrystalline AlCuLi [48]. As is often the case with the most interesting materials, only small samples were available. Measurements were made on a high-quality quasicrystalline parallelepiped of dimensions $0.6 \times 0.4 \times 0.4$ mm^3 to test the prediction that these materials should be elastically isotropic [49]. A measure of elastic anisotropy ε is given by

$$\varepsilon = 1 - 2C_{44}/(C_{11} - C_{12}). \tag{44}$$

For elastically isotropic materials $C_{44} = \frac{1}{2}(C_{11} - C_{12})$ so $\varepsilon = 0$. Spoor *et al* [48] found $\varepsilon = 0.0002 \pm 0.0007$ for their quasicrystalline sample. This value is considerably smaller than that for tungsten ($\varepsilon = 0.007 \pm 0.002$), which has the smallest anisotropy parameter of any crystalline material. Even had large samples been available, it would have been extremely difficult to set such a low limit on ε using conventional techniques because three independent sound velocity measurements would have been required, and it is doubtful that the relative precision of the elastic constant measurements could have been maintained in this case.

In addition to the use of RUS to study structural phase transitions in high-temperature superconductors mentioned above, the technique has been used to determine the complete elastic constant matrix for several other superconductors [1, 2, 36, 50]. The technique is especially useful because large single crystals, needed for more conventional techniques, are frequently not available. In addition, the symmetry is usually tetragonal (six elastic constants) or orthorhombic (nine elastic constants) so the complete determination of the elastic constant matrix by conventional means would be extremely difficult. RUS has also been used to measure the elastic constants of several intermetallic compounds [51–54]. These measurements are useful for a variety of reasons. Some engineering applications use single crystals, thus it is important to know the single-crystal elastic constants in order to determine properties such as the angular dependence of Young's modulus and the shear modulus. Elastic constant measurements are also important for comparison with first-principles calculations. In another remarkable case both the elastic constants and the crystalline orientation were determined from RUS measurements on single-crystal tantalum [55].

5.4. Outlook

There is an interest in using RUS for measurements under rather extreme conditions of pressure and temperature [56–58]. High temperatures and pressures are of interest for

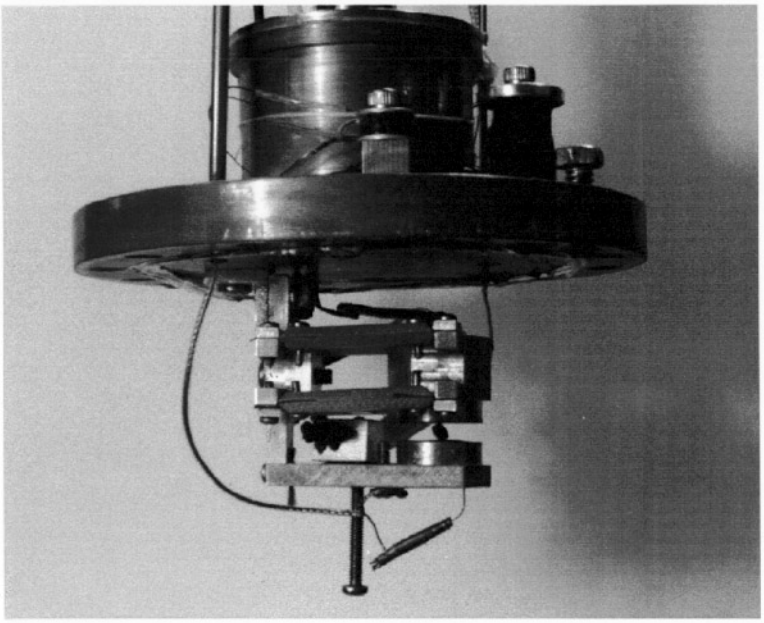

Figure 8. A photograph of a RUS sample–transducer assembly mounted in a ^{3}He cryostat. The sample, an $ScD_{0.19}$ parallelepiped, has room-temperature dimensions $1.498 \times 1.786 \times 1.999$ mm^3 with the largest dimension parallel to the hexagonal c axis.

geophysical studies—indeed, the early work in the development of RUS came from this area. A problem for the pressure-dependent studies is that the loading of the sample by the pressurizing gas strongly degrades the Q values of the resonance lines and shifts the frequencies at even moderate pressures [59]. This problem is not well understood. There is also an interest in using RUS at very low temperatures to investigate effects such as quantum-mechanical tunnelling of interstitials. We have made preliminary low-temperature measurements in a cryostat specially designed for RUS measurement. Figure 8 is a photograph of a sample mounted in a RUS probe [60] in a ^{3}He refrigerator. The sample, an $ScD_{0.19}$ parallelepiped, has room-temperature dimensions $1.498 \times 1.786 \times 1.999$ mm^3 with the largest dimension parallel to the hexagonal c axis. Figure 9 shows the resonant response of the $ScD_{0.19}$ parallelepiped at 296 mK. In another expansion of the use of RUS, magnetic systems are now being studied by the group of Albert Migliori at Los Alamos National Laboratory. In this case, some of the symmetries of the elastic constant matrix are lost due to the body torques exerted on the magnetic material.

RUS shows promise for the study of texture in polycrystalline materials. Processing often leads to a preferred orientation of the grains which results in a weak elastic anisotropy [61]. RUS is especially sensitive to this anisotropy because all elastic constants can be measured simultaneously. RUS has obvious potential for nondestructive testing because the eigenfrequencies depend on the shape of the material, and in fact on any variation of the density or elastic constants. By calculating the eigenmodes for specific shapes it is possible to understand which modes will be most sensitive to specific types of defect [62]. Finally, while the discussion and examples of this review have focused on solids, it is clear that the same principles apply to liquids.

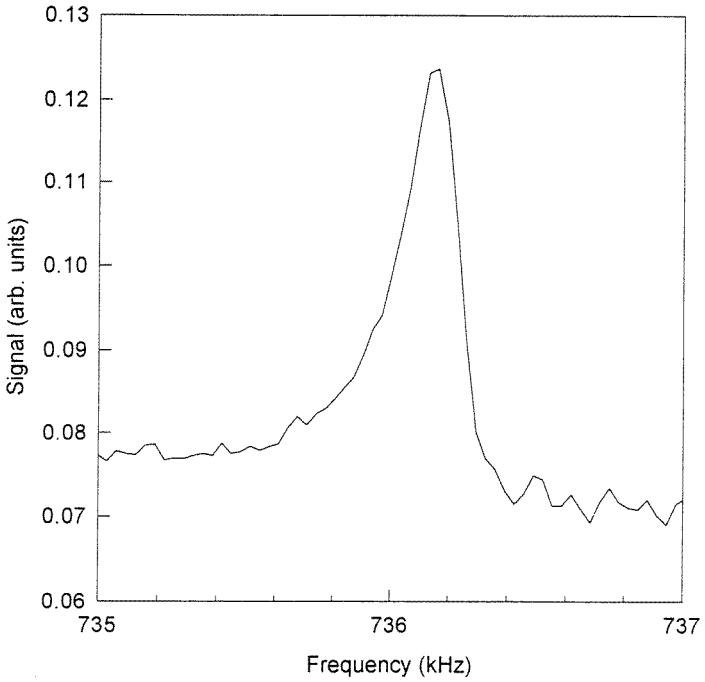

Figure 9. The resonant response of the $ScD_{0.19}$ parallelepiped of figure 8 at 296 mK.

6. Conclusions

Means have been developed to accurately measure the mechanical vibrational spectrum of physical objects, even quite small ones. It is also possible to efficiently calculate the vibrational eigenfrequencies of such objects if the shape, density, elastic constant matrix, and crystallographic orientation are known. With care, it is possible to solve the inverse problem, i.e. determine the material parameters from the measured frequencies. These capabilities underlie resonant ultrasound spectroscopy. RUS has been used to determine the complete elastic constant matrix for small ($\sim$1 mm^3) single crystals, even for materials with as many as nine independent elastic constants. This technique offers the promise of characterizing the elastic properties of new materials almost as routinely as one now characterizes the structure. It is also possible to obtain information about the dissipation associated with various symmetry strains. The full exploitation of this last possibility will result in an important new technique for the investigation of condensed matter. The sensitivity of the ultrasonic spectrum to such parameters as the shape of the sample points to many practical applications, several of which have already been realized.

Acknowledgments

The authors have benefited enormously from many discussions with Albert Migliori on all aspects of RUS. Keir Foster contributed to some of the measurements reported herein. This work was supported in part by a grant from the US National Science Foundation under No DMR-9501550.

References

[1] Migliori A, Visscher W M, Brown S E, Fisk Z, Cheong S W, Alten B, Ahrens E T, Kubat-Martin K A, Maynard J D, Huang Y, Kirk D R, Gillis K A, Kim H K and Chan M H W 1990 *Phys. Rev.* B **41** 2098
[2] Migliori A, Visscher W M, Wong S, Brown S E, Tanaka I, Kojima H and Allen P B 1991 *Phys. Rev. Lett.* **64** 2408
[3] Maynard J D 1992 *J. Acoust. Soc. Am.* **90** 1754
[4] Migliori A, Sarrao J L, Visscher W M, Bell T M, Lei M, Fisk Z and Leisure R G 1993 *Physica* B **183** 1
[5] Nye J F 1957 *Physical Properties of Crystals* (Oxford: Oxford University Press)
[6] Federov F I 1968 *Theory of Elastic Waves in Crystals* (New York: Plenum)
[7] Truell R, Elbaum C and Chick B B 1969 *Ultrasonic Methods in Solid State Physics* (New York: Academic)
[8] Bolef D I and Miller J G 1971 *Physical Acoustics VIII* ed W P Mason and R N Thurston (New York: Academic)
[9] Neighbours J M and Schacher G E 1967 *J. Appl. Phys.* **38** 5366
[10] Arístégui C and Baste S 1997 *J. Acoust. Soc. Am.* **101** 813
[11] Papadakis E P 1975 *Physical Acoustics XI* ed W P Mason and R N Thurston (New York: Academic)
[12] Stekel A, Sarrao J L, Bell T M, Ming L, Leisure R G, Visscher W M and Migliori A 1992 *J. Acoust. Soc. Am.* **92** 663
[13] Heyliger P, Jilani A, Ledbetter H, Leisure R G and Wang C-L 1993 *J. Acoust. Soc. Am.* **94** 1482
[14] Fraser D B and LeCraw 1964 *Rev. Sci. Instrum.* **35** 1113
[15] Spoor P S, White P J and Maynard J D 1996 *J. Acoust. Soc. Am.* **99** 2593
[16] Leisure R G, Migliori A and Schwarz R B 1992 *Perspectives in Physical Acoustics* ed Y Fu, R K Sundfors and P Suntharothok (Singapore: World Scientific)
[17] Kuokkala V-T and Schwarz R B 1992 *Rev. Sci. Instrum.* **63** 3136
[18] Dynamic Resonance Systems, Inc, 225 Lane 13, PO Box 1154, Powell, WY 82435, USA
[19] Quatrosonics, 4209 Balloon Park Road NE, Albuquerque, NM 87109, USA
[20] Holland R 1968 *J. Acoust. Soc. Am.* **43** 988
[21] Demarest H H 1971 *J. Acoust. Soc. Am.* **49** 768
[22] Ohno I 1976 *J. Phys. Earth* **24** 355
[23] Ohno I, Yamamoto S, Anderson O L and Noda J 1986 *J. Phys. C: Solid State Phys.* **47** 1103
[24] Visscher W M, Migliori A, Bell T M and Reinert R A 1991 *J. Acoust. Soc. Am.* **90** 2154
[25] Willis F 1996 *PhD Thesis* Colorado State University
[26] Press W H, Flannery B P, Teukolsky S A and Vetterling W T 1989 *Numerical Recipes* (Cambridge: Cambridge University Press)
[27] Leisure R G and Bolef D I 1967 *Phys. Rev. Lett.* **19** 957
[28] Leisure R G, Hsu D K and Seiber B A 1973 *Phys. Rev. Lett.* **30** 1326
[29] Sumino Y, Ohno I, Goto T and Kumazawa M 1976 *J. Phys. Earth* **24** 263
[30] Oda H, Isoda S, Inouye Y and Suzuki I 1994 *J. Geophys. Res.* **99** 15 517
[31] Landau L D and Liftshitz E M 1980 *Statistical Physics* (New York: Pergamon)
[32] Ting W, Fossheim K and Laegreid T 1990 *Solid State Commun.* **75** 727
[33] Krumhansl J A 1992 *Solid State Commun.* **84** 251
[34] Slonczewski J C and Thomas H 1970 *Phys. Rev.* B **1** 3599
[35] Rehwald W 1973 *Adv. Phys.* **22** 721
[36] Sarrao J L, Mandrus D, Migliori A, Fisk Z, Tanaka I, Kojima H, Canfield P C and Kodali P D 1994 *Phys. Rev.* B **50** 13 125
[37] Bussmann-Holder A, Migliori A, Fisk Z, Sarrao J L, Leisure R G and Cheong S-W 1991 *Phys. Rev. Lett.* **67** 513
[38] Willis F, Leisure R G and Kanashiro T 1996 *Phys. Rev.* B **54** 9077
[39] Imry J 1975 *J. Phys. C: Solid State Phys.* **8** 567
[40] Leisure R G, Schwarz R B, Migliori A and Lei M 1993 *Phys. Rev.* B **48** 1276
[41] Willis F, Leisure R G and Jacob I 1994 *Phys. Rev.* B **50** 13 792
[42] Leisure R G, Schwarz R B, Migliori A, Torgeson D R, Svare I and Anderson I S 1993 *Phys. Rev.* B **48** 887
[43] Leisure R G, Schwarz R B, Migliori A, Torgeson D R and Svare I 1993 *Phys. Rev.* B **48** 893
[44] Leisure R G, Schwarz R B, Migliori A, Torgeson D R, Svare I and Anderson I S 1993 *Z. Phys. Chem.* **179** S359
[45] Jäckle J 1972 *Z. Phys.* **257** 212
[46] Drescher-Krasicka E and Granato A V 1985 *J. Physique Coll.* **46** C10 73
[47] Kagan Y 1992 *J. Low Temp. Phys.* **87** 507

[48] Spoor P S, Maynard J D and Kortan A R 1995 *Phys. Rev. Lett.* **75** 3462
[49] Bak P 1986 *Phys. Rev.* B **32** 5764
[50] Lei M, Sarrao J L, Visscher W M, Bell T M, Thompson J D, Migliori A, Welp U W and Veal B W 1993 *Phys. Rev.* B **47** 6154
[51] Yasuda H and Koiwa M 1991 *J. Phys. Chem. Solids* **52** 723
[52] Yasuda H, Takasugi T and Koiwa M 1992 *Acta Metall. Mater.* **40** 381
[53] Mitchell T E, Chu F and Lei M 1994 *Phil. Mag* B **70** 867
[54] He Y, Schwarz R B, Migliori A and Whang S H 1995 *J. Mater. Res.* **10** 1187
[55] Sarrao J L, Chen S R, Visscher W M, Lei M, Kocks U F and Migliori A 1994 *Rev. Sci. Instrum.* **65** 2139
[56] Ohno I 1996 *J. Acoust. Soc. Am.* **99** 2579
[57] Anderson O L, Cynn H and Isaak D G 1996 *J. Acoust. Soc. Am.* **99** 2579
[58] Suzuki I, Fujio T, Kikuchi H, Oda H and Ohno I 1996 *J. Acoust. Soc. Am.* **99** 2580
[59] Isaak D G, Anderson O L, Carnes J D and Cynn H 1996 *J. Acoust. Soc. Am.* **99** 2579
[60] Designed by Albert Migliori
[61] Hirao M, Aoki K and Fukuoka H 1987 *J. Acoust. Soc. Am.* **81** 1434
[62] Lei M 1996 *J. Acoust. Soc. Am.* **99** 2593